JACS

Communication

Synthesis and Optical Properties of Lead-Free Cesium Tin Halide Perovskite Nanocrystals

Tom C. Jellicoe, Johannes M. Richter, Hugh F. J. Glass, Maxim Tabachnyk, Ryan Brady, Siân E. Dutton, Akshay Rao, Richard H. Friend, Dan Credgington, Neil C. Greenham, and Marcus L. Böhm*

Cavendish Laboratory, University of Cambridge, J.J. Thomson Avenue, Cambridge, CB3 0HE, United Kingdom

S *Supporting Information*

ABSTRACT: Metal halide perovskite crystal structures have emerged as a class of optoelectronic materials, which combine the ease of solution processability with excellent optical absorption and emission qualities. Restricting the physical dimensions of the perovskite crystallites to a few nanometers can also unlock spatial confinement effects, which allow large spectral tunability and high luminescence quantum yields at low excitation densities. However, the most promising perovskite structures rely on lead as a cationic species, thereby hindering commercial application. The replacement of lead with nontoxic alternatives such as tin has been demonstrated in bulk films, but not in spatially confined nanocrystals. Here, we synthesize $CsSnX_3$ (X = Cl, $Cl_{0.5}Br_{0.5}$, Br, $Br_{0.5}I_{0.5}$, I) perovskite nanocrystals and provide evidence of their spectral tunability through both quantum confinement effects and control of the anionic composition. We show that luminescence from Sn-based perovskite nanocrystals occurs on pico- to nanosecond time scales via two spectrally distinct radiative decay processes, which we assign to band-to-band emission and radiative recombination at shallow intrinsic defect sites.

During recent years solution-processable metal-halide perovskite semiconductors have shown tremendous potential in the field of optoelectronic devices including solar cells,[1,2] light-emitting diodes (LEDs),[3] and lasers.[4,5] This progress has been spurred by their excellent optical properties (i.e., sharp absorption edge[6] and high photoluminescence quantum yields[4]) and the prospect for low-cost device fabrication through cheap and versatile spin-casting, dip-coating, and evaporation methods.[1,7] Additionally, metal halide perovskites offer considerable tunability of the optical bandgap by integrating different halides into the crystal structure[8] or reducing the crystallite size to the nanometer scale.[9,10] While the first effect relies on the different ionization potentials of the various halide components, the second phenomenon is unlocked in quantum-confined nanostructures where the optical bandgap increases as the size is reduced.[11,12] Furthermore, the confinement of electrons and holes in these nanostructures promotes efficient radiative recombination compared to the bulk material. Consequently, at modest excitation densities the photoluminescence quantum efficiency (PLQE) for perovskite nanocrystals can be much higher than for bulk films of the same material,[4,9] which is particularly advantageous for achieving low lasing thresholds[5] and highly efficient LEDs.[13]

Although the performance of perovskite-based optoelectronics is impressive for such a young technology, the toxicity of the heavy metal component in current perovskite-based devices limits their large-scale commercial prospects. As a result, there has been a great deal of interest in replacing lead with nontoxic metals such as tin, bismuth, and germanium.[14−16] However, these lead-free perovskite materials are rather unstable under ambient conditions and produce lower device performances compared to their lead-containing analogues,[17] which has been ascribed to their higher defect densities.[18−20] In addition, no nanostructured Sn-based perovskites which exploit spatial confinement effects have been demonstrated. Here, we report the synthesis and optical characterization of $CsSnX_3$ (X = Cl, $Cl_{0.5}Br_{0.5}$, Br, $Br_{0.5}I_{0.5}$, I) perovskite nanocrystals, which utilize both compositional tuning and spatial confinement to adjust the bandgap from 2.8 to 1.3 eV, thereby spanning the visible to near-infrared region. Furthermore, using transient photoluminescence (PL) spectroscopy techniques, we analyze the decay dynamics in the pico- and nanosecond regime.

Synthesis of $CsSnX_3$ (X = Cl, $Cl_{0.5}Br_{0.5}$, Br, $Br_{0.5}I_{0.5}$, I) perovskite nanocrystals from Cs_2CO_3 and SnX_2 following literature methods for the analogous lead-based perovskite particles[9] was unsuccessful and led to the precipitation of CsX (see SI S2). In order to prevent such a reactant precipitation during particle synthesis, we prepared the tin precursor by dissolving SnX_2 in the mildly reducing and coordinating solvent tri-*n*-octylphosphine. This solution was then injected into a Cs_2CO_3 precursor solution containing oleic acid and oleylamine at 170 °C to obtain colloidally stable $CsSnX_3$ nanocrystals (see SI S1 for full experimental details). In Figure 1a we show powder X-ray diffraction (PXRD) patterns for the resulting $CsSnX_3$ (X = Cl, $Cl_{0.5}Br_{0.5}$, Br, $Br_{0.5}I_{0.5}$, I) particles. Rietveld refinement[21] confirms that all nanocrystal species adopt the perovskite structure (see SI S3). While chloride ions produce a cubic space group (*Pm*3*m*), we find that both bromide and iodide form perovskite crystal structures of lower symmetry (orthorhombic (*Pnma*)). This is consistent with literature findings for the parent bulk material where similar space groups have been reported, and where the cubic phase is the high-temperature state for all compounds.[22] We note that it was challenging to identify the precise space group for the
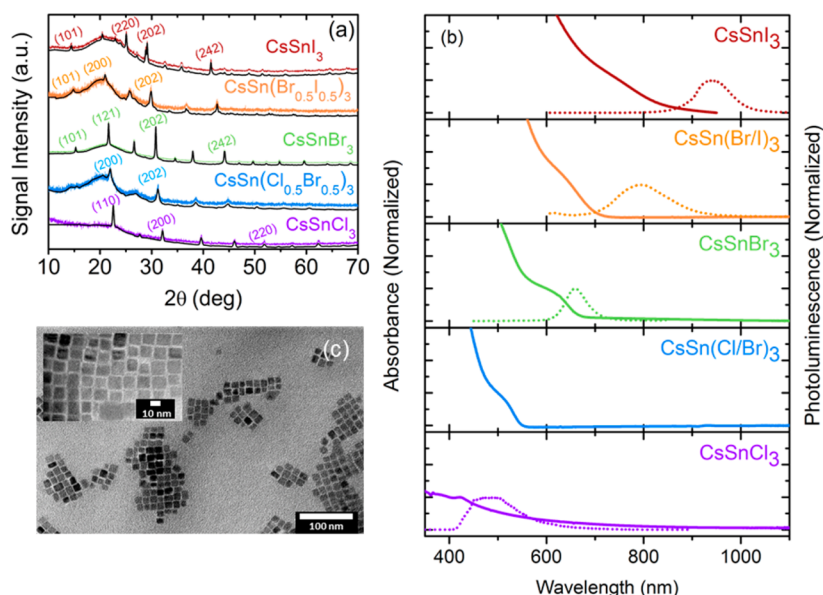
Figure 1. (a) PXRD spectra of $CsSnX_3$ (X = Cl, $Cl_{0.5}Br_{0.5}$, Br, $Br_{0.5}I_{0.5}$, I) perovskite nanocrystals. (b) Absorbance and steady-state PL of nanocrystals containing pure and mixed halides. The PL spectrum of $CsSn(Cl_{0.5}Br_{0.5})_3$ particles was identical to the pure chloride-containing nanocrystals and is shown in the SI S4. (c) TEM image of $CsSnI_3$ nanocrystals. Additional TEM images can be found in the SI S5.

mixed halide perovskite particles due to less intense and broader reflections (see Figure 1a).

Absorbance and PL measurements of the as-synthesized perovskite nanocrystals in solution and under inert atmosphere revealed optical bandgaps extending from the visible to the near-IR region (see Figure 1b). As is observed for the bulk materials, the bandgaps of tin-containing perovskite nanocrystals are red-shifted compared to analogous lead-based particles,[23] most likely due to the higher electronegativity of the tin ion occupying the 'B' site in the ABX_3 perovskite structure.[16] Compositional changes of the halide component allowed tuning of the optical bandgap, as has been shown for $APbX_3$ perovskite nanoparticles (see Figure 1b).[8,9,24] In addition to varying the halide ratio of the SnX_2 precursor during synthesis, the halide composition can also be adjusted postsynthetically via an anion-exchange reaction using different, pure-halide nanocrystals. This is consistent with previous reports on the lead-based perovskite particles (see SI S1 and S7).[8,9,24] The optical properties of these mixed halide particles are in agreement with statistical mixing between the halide species, indicated by highly disordered halide sites in the perovskite crystal lattice (see SI S8 for full PXRD analysis). In contrast to their lead analogues, the measured PLQEs are rather low (max 0.14%, see SI S6).

In addition to compositional tuning, adjusting the reaction temperature in the $CsSnBr_3$ nanocrystal synthesis between 125 and 170 °C allowed the optical bandgap to be tuned from 630 to 680 nm. This is consistent with weak quantum confinement for different sized $CsSnBr_3$ perovskite nanocrystals (see Figure 2). We note that particles synthesized at temperatures below 170 °C produced colloidally stable nanocrystals, however, postsynthetic purification resulted in particle dispersions showing similar optical properties to those of particles synthesized at 170 °C. This inability to produce purified particle dispersions prevented us from determining an accurate particle size via transmission electron microscopy (TEM).
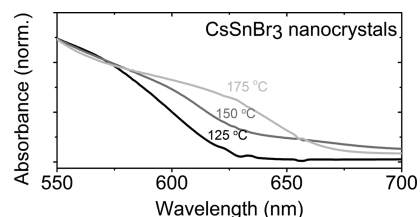

Figure 2. Absorbance profile of unpurified $CsSnBr_3$ perovskite nanocrystals synthesized at different temperatures.

To understand the optical properties of as-synthesized tin-based nanocrystals, we perform transient PL experiments on solution-dispersed particles. We use time-correlated single-photon counting (TCSPC) as well as measurements employing an electrically gated intensified CCD detector (ICCD) to spectrally resolve the PL kinetics in the pico- and nanosecond regime. Short- and long-time PL emission spectra, and characteristic decay kinetics, are presented in Figure 3 as well as in SI S9−S11. We note that all samples were colloidally stable within the time frame of measurements (up to 2 weeks). At longer times we observe that some particles precipitated which is most likely due to the dynamic character of ligand absorption and desorption processes,[25] which ultimately compromise colloidal stability in neat solvent over time.

For all nanocrystal compositions we observe a slight redshift of the PL spectrum over time (5−50 nm; see Figure 3a). Note that $CsSn(Cl_{0.5}Br_{0.5})_3$ particles show similar decay kinetics and spectral shifts to the $CsSnCl_3$ sample (see SI S4). This is consistent with a mixed halide phase which is nonemissive (e.g., due to anion disorder; see SI S8) and a very weak emission originating from a small subset of pure $CsSnCl_3$ nanocrystals only.[8]

Examining the kinetics of the PL of as-synthesized samples in the pico- and nanosecond regime reveals two distinct components, which decay on different time scales (see Figure 3b and SI S10). We note that fluence-dependent TCSPC measurements indicate that at the excitation densities
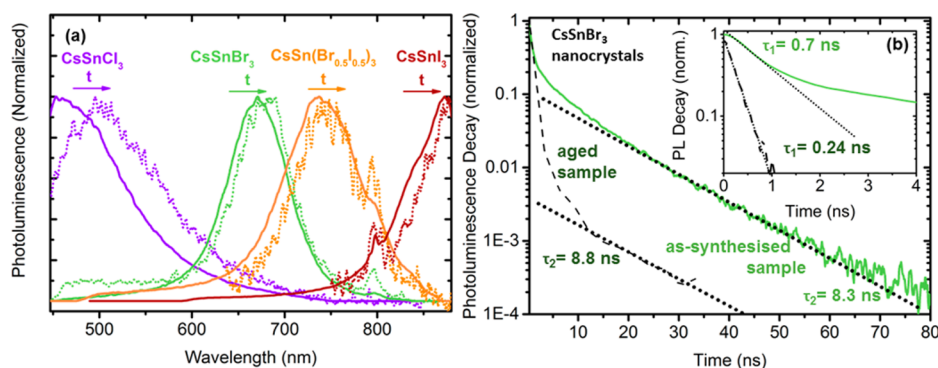
Figure 3. (a) PL of as-synthesized $CsSnX_3$ (X = Cl, Br, $Br_{0.5}I_{0.5}$, I) perovskite nanocrystals in solution after an ultrashort excitation (<ps) at 400 nm. The colored solid lines represent the integrated PL from 0 to 5 ns for each sample. Dashed lines are the integrated PL at time-slices of 30–60 ns ($CsSnCl_3$), 5–8 ns ($CsSnBr_3$), 30–50 ns ($CsSn(Br_{0.5}I_{0.5})_3$), and 8–30 ns ($CsSnI_3$). Further spectrally resolved PL decay data is shown in the SI S9. (b) Fast (inset) and slow PL decay kinetics of as-synthesized and aged $CsSnBr_3$ nanocrystals in solution, excited at 490 nm, and detected at 590–900 nm. The decay times have been determined using a biexponential (see SI S10). The fits are indicated as dashed black lines.

employed, both decay processes are dominated by mono-molecular decay kinetics (see SI S11). To determine the time constants of these decay processes, we use a biexponential fitting routine (see SI S10 for further details). For the chloride-containing nanocrystals the characteristic time scales are around 4 and 12 ns for the fast and slow components, respectively, and both processes are faster in samples containing heavier halides: 0.7 and 8 ns for $CsSnBr_3$, 0.3 and 3.3 ns for $CsSn(Br_{0.5}I_{0.5})_3$, and 0.3 and 2.6 ns for $CsSnI_3$. Furthermore, measuring the PL evolution of the same batch of dispersed nanocrystals after storing in an argon-filled glovebox for 1 week results in an accelerated faster decay component, which dominates the overall decay kinetics. The decay constant for the slower component remains unchanged in both aged and as-synthesized samples (see Figure 3b). Interestingly, we also find a significant reduction in PLQE when the luminescence quantum yield of as-synthesized nanocrystals was remeasured after 1 week of storage under inert gas. We note that X-ray photoelectron spectroscopy (XPS) measurements conducted in parallel indicate only very small compositional changes over time and no evidence for extensive particle oxidation (see SI S12). If the particles, however, are exposed to the ambient only briefly (ca. 5 min), we observe a small spectral shift of the tin binding energy toward higher values which is consistent with an oxidation process from Sn(II) to Sn(IV) (see SI S13).[26] This change in oxidation state is accompanied by a drop in PL efficiency to nondetectable values (<0.01% PLQE).

Considering the spectral red-shift of the luminescence within a few nanoseconds and the two different PL decay processes, we suggest that the fast-decaying luminescence of as-synthesized Sn-based perovskite nanocrystals originates from band-edge states, while the slower decay is due to recombination from states just below the band edge. Such shallow states within the bandgap are likely to arise from the intrinsic defect sites which are common in Sn-based perov-skites.[17,27] Two possible scenarios can produce such a PL decay: First, a subset of defect-free nanocrystals producing fast band-to-band emission while the remaining defect-containing particles show a slower, spectrally red-shifted PL decay profile or, second, a homogeneous population of particles where trapping at defects competes with band-to-band emission followed by red-shifted emission from defect sites. The first scenario has been discussed as an explanation for similar PL kinetics observed in other nanocrystal systems.[28,29] Considering

an average nanocrystal volume of ~10^{-18} cm^3, such decay behavior would require intrinsic defect state densities of Sn-based perovskite nanocrystals on the order of ~10^{17} cm^{-3}. Interestingly, similar defect densities have been reported for the parental bulk materials.[30,31] We note that such an effect may not be observable in Pb-based perovskite nanocrystals as significantly lower defect densities have been reported for lead-containing perovskites,[4,6,20,24] thereby rendering a detection of any red-shifted defect emission more difficult than in $CsSnX_3$ nanocrystals.

Furthermore, the formation energy of defects in Sn-based perovskites is relatively low (~250 meV) which provides considerable driving force toward the formation of defect densities as high as ~10^{19} cm^{-3} over time.[31] Some of these defects have been shown to create trap states in the middle of the bandgap.[31] Population of these deep acceptor states can be fast (sometimes only a few hundred picoseconds),[32] and recombination from these states is mostly nonradiative.[33]

We therefore interpret our observation of an accelerated fast PL decay component for particles stored under inert atmosphere for 1 week (see Figure 3b) and the accompanied quench in PLQE as the consequence of nonradiative decay at deep acceptor states which have been developed slowly after synthesis. The formation of such deep acceptor sites can be produced by very subtle structural rearrangements[33] which may not be detectable in our XPS measurements. It is interesting that the lifetime of the slower decay component in the inert gas atmosphere-aged samples remains unchanged, suggesting that there is still some population of nanocrystals which emit from shallow intrinsic defect sites that are not affected by the new nonradiative decay. The undetectable luminescence yield after exposure to the ambient environment is most likely due to the creation of nonradiative defect states deep in the bandgap of oxidized perovskite structures.[27]

In conclusion, we successfully synthesized $CsSnX_3$ (X = Cl, $Cl_{0.5}Br_{0.5}$, Br, $Br_{0.5}I_{0.5}$, I) nanocrystals and confirm their underlying perovskite crystal structure. We tuned the optical bandgap throughout the near-infrared and visible spectral region using both quantum confinement effects and employing different halides in the perovskite crystal. Furthermore, we highlight two different approaches to produce mixed halide perovskite structures by either directly synthesizing the nanostructure using different halide sources or applying a postsynthetic anion exchange reaction by mixing as-synthesized

pure-halide perovskite particles. Resolving the temporal and spectral evolution of the PL of Sn-based perovskite nanocrystals reveals two luminescent decay channels, which we assign to a fast band-to-band emission and slow radiative recombination at shallow intrinsic defect sites.

■ ASSOCIATED CONTENT

Ⓢ Supporting Information

The Supporting Information is available free of charge on the ACS Publications website at DOI: 10.1021/jacs.5b13470.

> Experimental details and data (PDF)
> The data underlying this publication are available at https://www.repository.cam.ac.uk/handle/1810/254023

■ AUTHOR INFORMATION

Corresponding Author

*mb842@cam.ac.uk

Notes

The authors declare no competing financial interest.

■ ACKNOWLEDGMENTS

■ REFERENCES

(1) Lee, M. M.; Teuscher, J.; Miyasaka, T.; Murakami, T. N.; Snaith, H. J. *Science* **2012**, *338*, 643.

(2) Jeon, N. J.; Noh, J. H.; Yang, W. S.; Kim, Y. C.; Ryu, S.; Seo, J.; Seok, S. Il. *Nature* **2015**, *517*, 476.

(3) Tan, Z.-K.; Moghaddam, R. S.; Lai, M. L.; Docampo, P.; Higler, R.; Deschler, F.; Price, M.; Sadhanala, A.; Pazos, L. M.; Credgington, D.; Hanusch, F.; Bein, T.; Snaith, H. J.; Friend, R. H. *Nat. Nanotechnol.* **2014**, *9*, 687.

(4) Deschler, F.; Price, M.; Pathak, S.; Klintberg, L. E.; Jarausch, D. D.; Higler, R.; Hüttner, S.; Leijtens, T.; Stranks, S. D.; Snaith, H. J.; Atatüre, M.; Phillips, R. T.; Friend, R. H. *J. Phys. Chem. Lett.* **2014**, *5*, 1421.

(5) Yakunin, S.; Protesescu, L.; Krieg, F.; Bodnarchuk, M. I.; Nedelcu, G.; Humer, M.; De Luca, G.; Fiebig, M.; Heiss, W.; Kovalenko, M. V. *Nat. Commun.* **2015**, *6*, 8056.

(6) Sadhanala, A.; Deschler, F.; Thomas, T. H.; Dutton, S. E.; Goedel, K. C.; Hanusch, F. C.; Lai, M. L.; Steiner, U.; Bein, T.; Docampo, P.; Cahen, D.; Friend, R. H. *J. Phys. Chem. Lett.* **2014**, *5*, 2501.

(7) Liu, M.; Johnston, M. B.; Snaith, H. J. *Nature* **2013**, *501*, 395.

(8) Nedelcu, G.; Protesescu, L.; Yakunin, S.; Bodnarchuk, M. I.; Grotevent, M. J.; Kovalenko, M. V. *Nano Lett.* **2015**, *15*, 5635.

(9) Protesescu, L.; Yakunin, S.; Bodnarchuk, M. I.; Krieg, F.; Caputo, R.; Hendon, C. H.; Yang, R. X.; Walsh, A.; Kovalenko, M. V. *Nano Lett.* **2015**, *15*, 3692.

(10) Di, D.; Musselman, K. P.; Li, G.; Sadhanala, A.; Ievskaya, Y.; Song, Q.; Tan, Z.-K.; Lai, M. L.; MacManus-Driscoll, J. L.; Greenham, N. C.; Friend, R. H. *J. Phys. Chem. Lett.* **2015**, *6*, 446.

(11) Alivisatos, A. P. *Science* **1996**, *271*, 933.

(12) Böhm, M. L.; Jellicoe, T. C.; Rivett, J.; Sadhanala, A.; Davis, N. J. L. K.; Morgenstern, F. S. F.; Goedel, K. C.; Govindasamy, J.; Benson, C. G. M.; Greenham, N. C.; Ehrler, B. *J. Phys. Chem. Lett.* **2015**, *6*, 3510.

(13) Dai, X.; Zhang, Z.; Jin, Y.; Niu, Y.; Cao, H.; Liang, X.; Chen, L.; Wang, J.; Peng, X. *Nature* **2014**, *515*, 96.

(14) Marshall, K. P.; Walton, R. I.; Hatton, R. A. *J. Mater. Chem. A* **2015**, *3*, 11631.

(15) Park, B.-W.; Philippe, B.; Zhang, X.; Rensmo, H.; Boschloo, G.; Johansson, E. M. J. *Adv. Mater.* **2015**, *27*, 6806.

(16) Chen, Q.; De Marco, N.; Yang, Y.; Song, T.-B.; Chen, C.-C.; Zhao, H.; Hong, Z.; Zhou, H.; Yang, Y. *Nano Today* **2015**, *10*, 355.

(17) Noel, N. K.; Stranks, S. D.; Abate, A.; Wehrenfennig, C.; Guarnera, S.; Haghighirad, A.-A.; Sadhanala, A.; Eperon, G. E.; Pathak, S. K.; Johnston, M. B.; Petrozza, A.; Herz, L. M.; Snaith, H. J. *Energy Environ. Sci.* **2014**, *7*, 3061.

(18) Takahashi, Y.; Obara, R.; Lin, Z.-Z.; Takahashi, Y.; Naito, T.; Inabe, T.; Ishibashi, S.; Terakura, K. *Dalton Trans.* **2011**, *40*, 5563.

(19) Takahashi, Y.; Hasegawa, H.; Takahashi, Y.; Inabe, T. *J. Solid State Chem.* **2013**, *205*, 39.

(20) Kumar, M. H.; Dharani, S.; Leong, W. L.; Boix, P. P.; Prabhakar, R. R.; Baikie, T.; Shi, C.; Ding, H.; Ramesh, R.; Asta, M.; Graetzel, M.; Mhaisalkar, S. G.; Mathews, N. *Adv. Mater.* **2014**, *26*, 7122.

(21) Rietveld, H. M. *J. Appl. Crystallogr.* **1969**, *2*, 65.

(22) Scaife, D. E.; Weller, P. F.; Fisher, W. G. *J. Solid State Chem.* **1974**, *9*, 308.

(23) Hao, F.; Stoumpos, C. C.; Cao, D. H.; Chang, R. P. H.; Kanatzidis, M. G. *Nat. Photonics* **2014**, *8*, 489.

(24) Akkerman, Q. A.; D'Innocenzo, V.; Accornero, S.; Scarpellini, A.; Petrozza, A.; Prato, M.; Manna, L. *J. Am. Chem. Soc.* **2015**, *137*, 10276.

(25) De Roo, J.; Ibáñez, M.; Geiregat, P.; Nedelcu, G.; Walravens, W.; Maes, J.; Martins, J. C.; Van Driessche, I.; Kovalenko, M. V.; Hens, Z. *ACS Nano* **2016**, *10*, 2071.

(26) Kwoka, M.; Ottaviano, L.; Passacantando, M.; Santucci, S.; Czempik, G.; Szuber, J. *Thin Solid Films* **2005**, *490*, 36.

(27) Xiao, Z.; Zhou, Y.; Hosono, H.; Kamiya, T. *Phys. Chem. Chem. Phys.* **2015**, *17*, 18900.

(28) Ebenstein, Y.; Mokari, T.; Banin, U. *Appl. Phys. Lett.* **2002**, *80*, 4033.

(29) Pons, T.; Medintz, I. L.; Farrell, D.; Wang, X.; Grimes, A. F.; English, D. S.; Berti, L.; Mattoussi, H. *Small* **2011**, *7*, 2101.

(30) Chung, I.; Song, J. H.; Im, J.; Androulakis, J.; Malliakas, C. D.; Li, H.; Freeman, A. J.; Kenney, J. T.; Kanatzidis, M. G. *J. Am. Chem. Soc.* **2012**, *134*, 8579.

(31) Xu, P.; Chen, S.; Xiang, H.-J.; Gong, X.-G.; Wei, S.-H. *Chem. Mater.* **2014**, *26*, 6068.

(32) Bakulin, A. A.; Neutzner, S.; Bakker, H. J.; Ottaviani, L.; Barakel, D.; Chen, Z. *ACS Nano* **2013**, *7*, 8771.

(33) Voznyy, O.; Thon, S. M.; Ip, a. H.; Sargent, E. H. *J. Phys. Chem. Lett.* **2013**, *4*, 987.